Jpn J Ophthalmol 2010;54:349–356
DOI 10.1007/s10384-010-0826-9


LABORATORY INVESTIGATION

# Novel Snapshot Imaging of Photoreceptor Bleaching in Macaque and Human Retinas

Yoko Kazato[1,2,3], Naohisa Shibata[4], Gen Hanazono[1,2,5], Wataru Suzuki[1,2], Manabu Tanifuji[2], and Kazushige Tsunoda[1,2]

[1] Laboratory of Visual Physiology, National Institute of Sensory Organs, Tokyo, Japan; [2] Laboratory for Integrative Neural Systems, Brain Science Institute, Riken, Saitama, Japan; [3] Department of Ophthalmology, Nihon University School of Medicine, Tokyo, Japan; [4] Nidek Co., LTD., Aichi, Japan; [5] Department of Ophthalmology, Kikkoman General Hospital, Chiba, Japan

**Abstract**

**Purpose:** Various methods have been used to obtain a topographic map of bleached photopigments in human retinas in the past. The purpose of this study was to determine whether the bleaching topography of the photoreceptors could be obtained by snapshot imaging reflectometry.

**Methods:** Four to five fundus photographs of one rhesus monkey and three healthy human subjects were taken by white flashes at intervals of 4 s, with a commercial fundus camera with minimal modifications. The flash-induced reflectance increases (bleaching) were calculated by dividing the reflectance of the first image into the subsequent images, pixel by pixel.

**Results:** The topography of the bleached macula corresponded well with the anatomical distribution of the cones. The ratio of reflectance changes in the center to that in the surrounding tissue was high for red and low for green and blue images. These results indicate that the reflectivity changes were not artifacts but were derived from changes in the photopigment density in the cones and rods.

**Conclusions:** The topography of bleached photoreceptors obtained with a commercial fundus camera from one monkey and three healthy human subjects showed that this technique has potential as a new clinical method for examining photoreceptor function in both normal and diseased retinas. **Jpn J Ophthalmol** 2010;54:349–356 © Japanese Ophthalmological Society 2010

**Keywords:** bleaching, densitometry, fundus camera, imaging reflectometry, snapshot photography

## Introduction

The morphology of the retina can be imaged with very high spatial resolution by recent imaging techniques such as scanning laser ophthalmoscopy (SLO)[1,2] and optical coherence tomography (OCT).[3,4] However, these imaging instruments do not allow objective assessment of retinal function, which is essential for making correct diagnoses of various retinal disorders. Because the quality of vision, such as visual acuity and visual fields, depends not only on the anatomical density of the photoreceptors but also on their neural function, mapping retinal responsiveness is important both from physiological and clinical points of view.

At present, the functional topography of cone-derived retinal responsiveness is obtained by multifocal electroretinograms (mfERGs) in the clinic,[5] but the spatial resolution of mfERGs is limited. Intrinsic signal imaging with infrared light[6–14] and functional OCT[15–17] has been used recently to map light scattering changes of the photoreceptors following neuronal activities. However, these techniques have not been brought into the clinic, mainly because of their low signal-to-noise ratios (SNRs).

Some 50 years ago, the bleaching of photopigments was determined quantitatively by measuring reflectance changes during the bleaching and regeneration processes in human retinas. This method was used to determine precisely the in

Received: July 29, 2009 / Accepted: February 24, 2010
Correspondence and reprint requests to: Kazushige Tsunoda, Laboratory of Visual Physiology, National Institute of Sensory Organs, 2-5-1 Higashigaoka, Meguro-ku, Tokyo 152-8902, Japan
e-mail: tsunodakazushige@kankakuki.go.jp

vivo kinetics of the photopigments in the cone and rod photoreceptors.[18–22] Retinal densitometry was later used to measure the spatial and spectral distribution of the reflectance changes by examining images obtained with either a fundus camera or by SLO, that is, by imaging fundus reflectometry.[14,23–31] These techniques allowed the investigators to map objectively and noninvasively the cones and rods as bleach-derived light reflectance changes in both normal and diseased eyes.

Imaging fundus reflectometry, however, has fundamental problems both theoretically and technically,[31,32] and it is not widely used in the clinic in spite of numerous reports published by different laboratories. One practical problem is that the recording period during which the subject must fixate a target steadily is long and uncomfortable. This is a common problem shared by many of the imaging techniques, such as OCT, that are used to study the ocular fundus. However, a much more critical problem in reflectometry measurements is that a small displacement of the fundus image during the long fixation period leads to a loss of important densitometric information.

To overcome this limitation, we measured the retinal reflectance changes by taking consecutive snapshot images with short duration flashes (<1.0 ms), and analyzing the density of corresponding areas of the retina, pixel by pixel, as a function of time. A topographic map of the bleached photoreceptors was obtained within 12 s from each of three healthy human subjects, and the reliability of the results was confirmed in an experiment on an anesthetized monkey. A commercial fundus camera with minimal modifications was used, and the bleaching topography was obtained by simple analyses of the images.

## Methods

### *Apparatus*

A slightly modified commercial fundus camera (AFC-210, NIDEK, Aichi, Japan) was used. The field of view covered 45° of the ocular fundus. To observe the fundus, light from a halogen lamp (Fig. 1B, I) was passed through an infrared interference filter (H) and the optical system of the camera (F, B, and A) to illuminate the retina, and the retinal image was monitored by the image on a charge-coupled device (CCD) camera. This image was used to adjust the field viewed and to focus on the retina before the recording. A small fixation target of a green light-emitting diode (LED), masked by a triangular pattern, was placed in the optical path (E). A movable mirror (C) was placed between the objective lens and the CCD camera, which was used to change the optical pathway either to the CCD camera for focusing or to a complementary metal oxide semiconductor (CMOS) camera for recording the images (EOS-5D, Canon, Tokyo, Japan). Just before the flash, the mirror was mechanically displaced for 1/50 s so that the retinal image could be photographed by the CMOS camera. A ring-shaped xenon strobe (G) (flash duration <1.0 ms) was placed in the optical pathway of the halogen lamp. The variation in the intensity of the xenon flash strobe was less than ±1.0%, which is negligible considering that the reflectance changes at the fovea were 20%–40% in the monkey and 15%–20% in the humans.

To enable more accurate fixation in this imaging reflectometric method, the fixation target was modified as follows: the circular mask for the fixation target was replaced by a triangular one, and the subjects were instructed to fixate on one apex of that triangle during the whole recording period. The intensity of the target illumination was set lower than the threshold level of bleaching in this system.

### *Data Analyses*

The raw images were first converted to TIFF images (350 dpi, 16 bit, 4368 × 2912 pixels) using Digital Photo Professional Ver. 2.1.1.4, developed by the manufacturer of the fundus camera. These images have separate information for blue, green, and red components of the images, which correspond to the three peak sensitivities of the CMOS: 460, 540, and 640 nm (Fig. 2, raw images). However, each of the spectral characteristics of the CMOS might not be equally converted to the TIFF image, and, unfortunately, the technical details of the color-image processing are not disclosed by the manufacturer. The peak sensitivities of the CMOS were measured with a spectral light source (OL490 Agile Light Source, Optronic Laboratories, Gooch & Housego, Melbourne, FL, USA).

In the human measurements, the alignment of consecutive images was performed by normalized grayscale correlation, to correct for misalignments of the retinal images due to eye movements ($x$–$y$ axes and rotation) before the differential analyses. When the location of the true correlation peak was being estimated, the alignment was improved by fitting an analytical model of the correlation peak based on a similarity interpolation estimation, which allowed for subpixel estimation. We applied the algorithm from the Matrox imaging library version 9.0 to estimate the exact position of the correlation peak with 0.01 pixel resolution. If the motion-derived displacements among the consecutive flashes were too large to be corrected by the off-line alignment, the data were discarded. The flash-induced reflectance increases (bleaching) were calculated by dividing the reflectance of the first image by the subsequent images, pixel by pixel (Fig. 2, differential images). These differential images were spatially smoothed by a simple moving average (32 × 32 pixels in monkey and 54 × 54 in human) to reduce the noise of the CMOS camera before the profile and the topographic images of bleaching were displayed. They were then separated into red, green, and blue components (Fig. 2).

### *Subjects and Recording Protocols*

Snapshot images were taken from one rhesus monkey (*Macaca mulatta*) and three healthy human subjects (subject

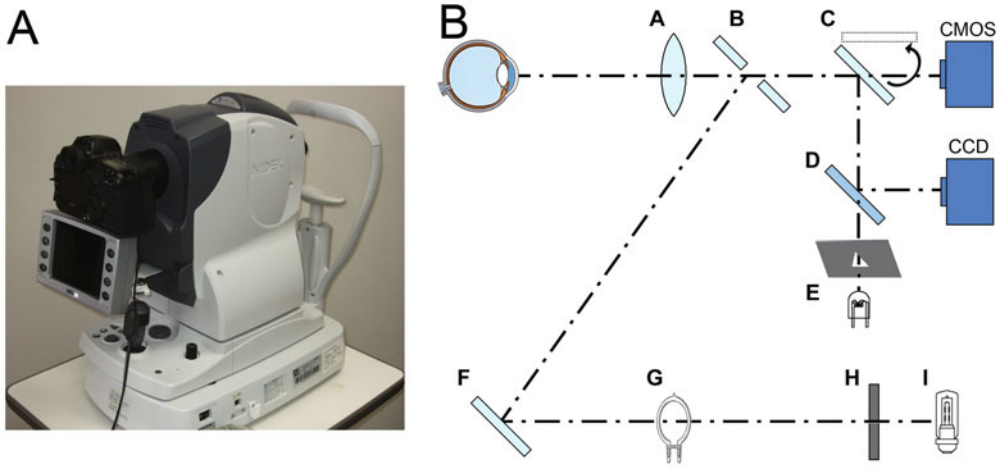


**Figure 1A, B.** Snapshot imaging reflectometry. **A** Fundus camera system used. **B** Schematic drawing of the optics. *A,* objective lens; *B,* pin-hole mirror; *C,* movable mirror; *D,* dichroic mirror; *E,* triangle-shaped fixation target with light-emitting diode; *F,* full reflection mirror; *G,* xenon flash strobe; *H,* infrared interference filter; *I,* halogen lamp; *CMOS*, complementary metal oxide semiconductor camera; *CCD*, charge-coupled device camera.

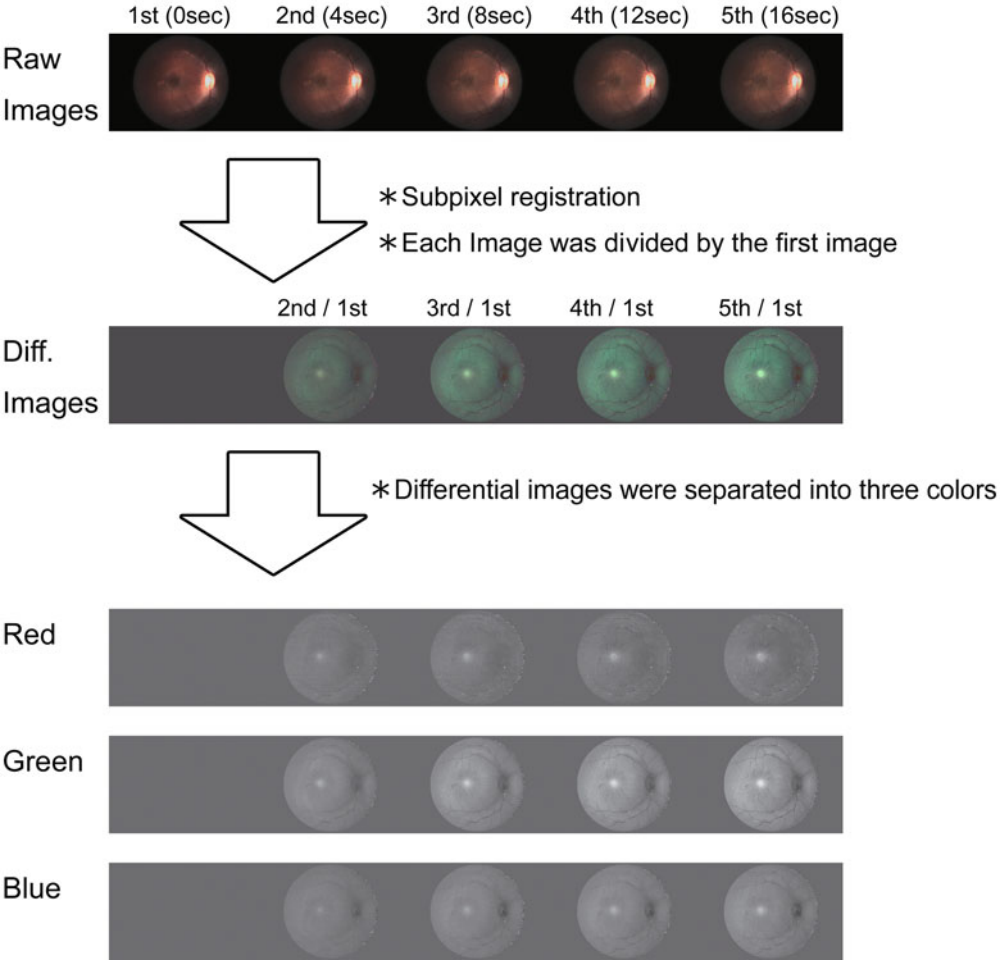


**Figure 2.** Consecutive snapshot images of the ocular fundus of a monkey. Following transformation to TIFF images, the raw images were realigned by subpixel registration, and differential images were obtained. The first image was used as a reference. The differential images were then separated into the three color components.

1, a 43-year-old man; subject 2, a 38-year-old man; and subject 3, a 33-year-old woman).

The experimental protocol for the monkey was approved by the Experimental Animal Committee of the RIKEN Institute, and all experimental procedures in animals were carried out in accordance with the guidelines of the institute. For the human experiments, the procedures used conformed to the tenets of the Declaration of Helsinki, and informed consent was obtained from each individual who participated in this study after an explanation of the procedures used. The project was approved by the Institutional Review Board of National Institute of Sensory Organs.

Jpn J Ophthalmol
Vol 54: 349–356, 2010

Monkeys were first injected intramuscularly with atropine sulfate (0.08 mg/kg) and then anesthetized with droperidol (0.25 mg/kg) and ketamine (5.0 mg/kg). The animals were paralyzed with vecuronium bromide (0.1–0.2 mg/kg per hour) to suppress eye movements, and artificially ventilated with a mixture of 70% $N_2O$, 30% $O_2$, and 1.0%–1.5% isoflurane. Electroencephalograms, electrocardiograms, expired $CO_2$, and rectal temperature were monitored continuously throughout the experiments. Before the recording, the pupils were fully dilated with topical tropicamide (0.5%) and phenylephrine hydrochloride (0.5%). After 30 min of dark adaptation, the retina was focused on the camera plane by observing the infrared images with the CCD camera. Then, five fundus photographs were taken by white flashes at 4-s intervals for a total of 16 s. The flash intensity was 101.0 cds/$m^2$.

The retinas of the human subjects were measured under room illumination without dark adaptation. Following pupillary dilation, each subject's head was stabilized on a head and chin rest. During the whole duration of the measurements, the subject fixated on one apex of a triangle, which was illuminated by a green LED. Four fundus photographs were taken by white flashes at 4-s intervals. The flash intensity was either 31.8 (subject 1) or 63.6 (subjects 2 and 3) cds/$m^2$.

## Results

In the monkey, the reflectance of the whole recording region of the retina was increased by the consecutive flashes (Fig. 3). The increase in the reflectance in all three colors always peaked at the fovea. The bleaching profiles of four consecutive images in red showed that the reflectance gradually increased at the fovea (15% in second/first and 23% in fifth/first images), whereas the increase was not apparent in the perimacular region at around 10° temporal to the fovea (Fig. 3, top right). The bleaching profiles for green and blue, on the other hand, showed that the reflectance gradually increased both at the fovea (20% in the second/first image and 40% in the fifth/first image for green), and in the perimacular region (10% in the second/first image and 20% in the fifth/first image for green) (Fig. 3, middle and bottom right).

The reflectance ratio of the central peak to the surrounding area (10° temporal to the fovea) in the fifth/first image was high for the red (3.3) and low for the green (2.0) and blue (1.8) images (Fig. 3, right). These results can be easily explained by the contribution of cone photoreceptors to the red image, and both cone and rod photoreceptors to the green and blue images. These findings are good evidence that reflectivity changes measured by this method are not artifacts but are derived from the photoreceptors.

It should be noted that the reflectance at the optic disc and part of the retinal vessels decreased following flashes. These are intrinsic signals that are derived from light scattering changes following blood flow increases.[7–10]

In the human subjects, only the data for green with the largest reflectance changes, are presented in Fig. 4. As in the monkey, the reflectance of the central region was increased by consecutive flashes. The bleaching topography in the macula corresponds well with the anatomical distribution of cones,[33,34] electrophysiological cone activity,[5] and psychophysical cone sensitivity. Because the images were taken without dark adaptation and under room illumination, the response in the perimacular region was not as prominent as in the monkey. The data from the human subjects were affected by eye-movement artifacts, and some noise from the retinal vessels and superficial reflexes may have affected the images, even following subpixel adjustment of the images (Fig. 4, subjects 2 and 3, arrows). It is notable that the intrinsic signal (light reflectance decrease) reflecting blood flow increases was clearly observed at the optic disc.[7–10]

## Discussion

We measured the reflectance changes of the ocular fundus by taking consecutive snapshots of the retina with a commercial fundus camera and obtained a topographic map of cone photoreceptors that corresponded to the density of the cones in normal retinas. Only a slight modification of a commercially available fundus camera, namely, the shape of the fixation target was changed, was made to reduce the eye and head movement during recording in order to obtain reliable photographs. The dental impression plate, commonly used in previous studies, was not needed for these measurements. Many different types of instruments have been used for imaging fundus reflectometry.[32,35] Early attempts were made with slightly modified conventional fundus cameras. These investigators compared photographic images on 35 mm film photographs before and after bleaching or photographs of locally bleached retina, by embedding masks in the light path to bleach selected areas of the retina.[14,23–25] The density contrast of rod photopigments was estimated both in normal subjects and in patients with night blindness; however, this method had inherent problems in calibration, and the topographic representation of cone or rod bleaching was not reliable.

Fundus reflectometry with video-based fundus cameras was later introduced.[26–29] The density map of cone photopigments corresponding to the anatomical distribution of the cones was obtained in humans,[26] and the rod-dominant photopigment density was also estimated from the peripheral retina.[27,28] However, the recording protocols were too complicated and the bleaching topographies obtained by these methods did not have enough image quality for clinical assessment of either the cone or rod photopigments.

SLO has also been used to measure bleach-related reflectance changes.[30,31] The confocal nature of SLO has the great advantage of reducing unwanted scattered light from the retinal surface, inevitable in fundus camera-based imaging reflectometry. The foveal cone density with a peak

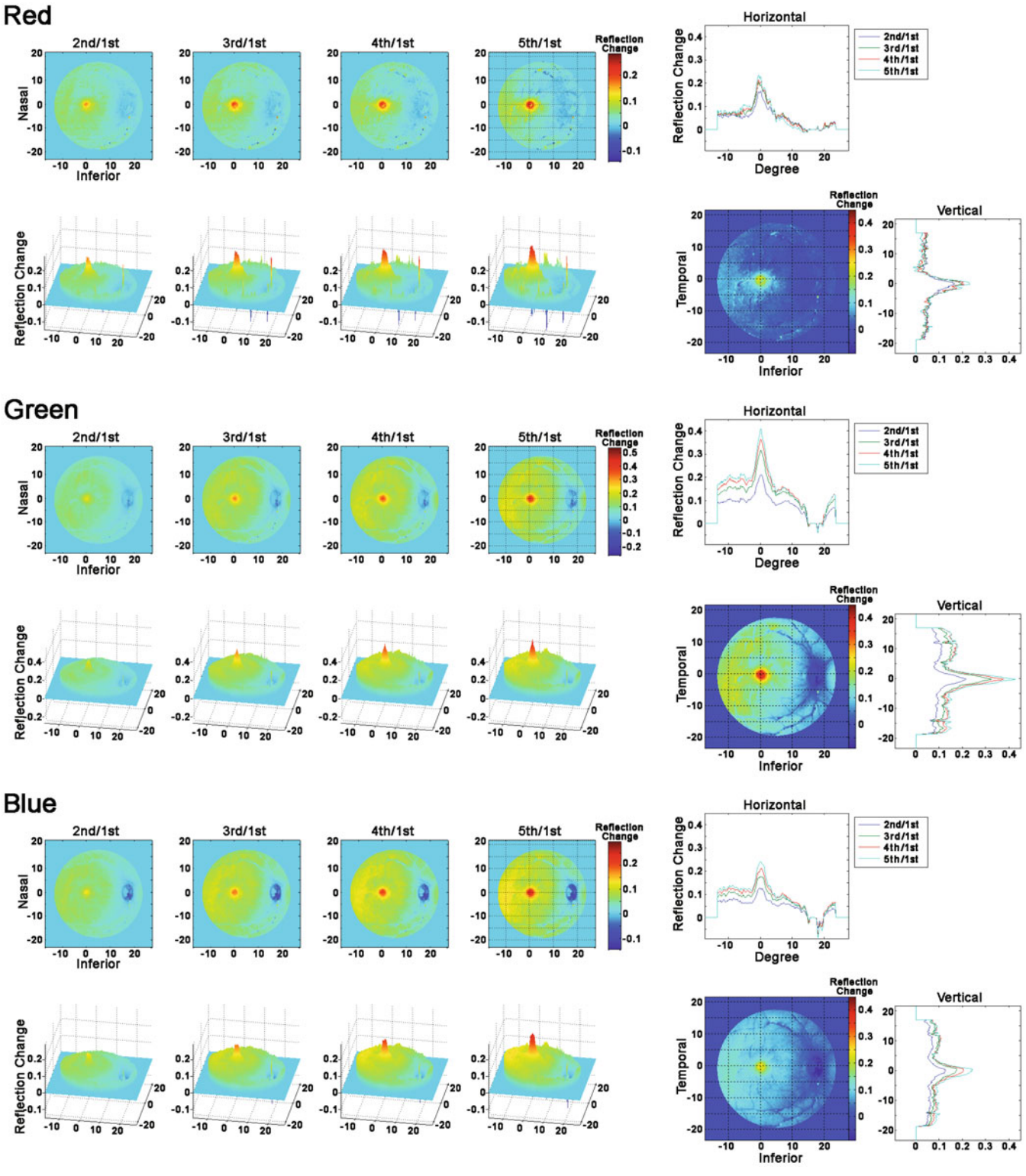


**Figure 3.** Pseudocolor topographies of the light reflectance changes in the right eye of a monkey for the three color components. Red and blue color scales indicate increased (brightening) and decreased (darkening) light reflectance, respectively. The horizontal and vertical profiles of the reflectance changes are shown on the right. The retinal images were cropped to the central 37°.

Jpn J Ophthalmol
Vol 54: 349–356, 2010

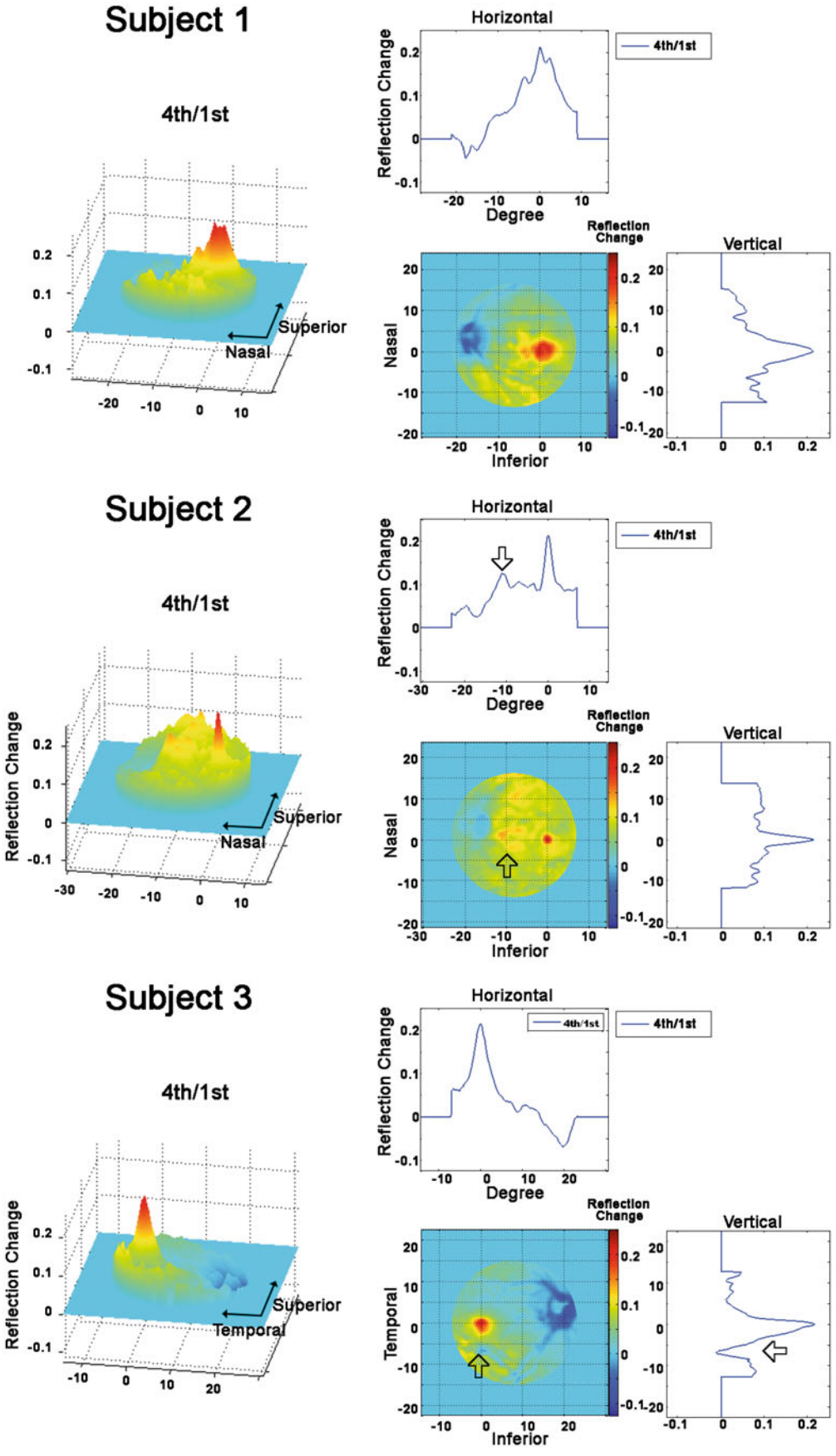


**Figure 4.** Pseudocolor topographies and horizontal and vertical profiles of the light reflectance changes in the three human subjects. Only the results of the fourth and the first image for the green component are shown. The red and blue color scales indicate light reflectance increases (brightening) and decreases (darkening), respectively. *Arrows* (subjects 2 and 3) indicate artifactual decreases or increases of light reflectance due to scattering from the superficial layer. The retinal images were cropped to the central 30°.

at the fovea is clearly evident in healthy subjects.[36] However, for mapping the distribution of the photopigments, the recording protocol is still too complicated, and the number of modifications that have to be made to the commercial instrument make it difficult to use in the clinic.[37]

Recently, changes in the intensity of fundus autofluorescence during bleaching have been used to assess photopigment distribution. However, the measured reflectivity is strongly affected by absorption of macular pigments, limiting its use.[38]

In our technique, the fundus images were obtained by consecutive photographs taken by short-duration flashes of identical intensity, and the pixel values of the consecutive images were compared with the initial referential image to extract the flash-evoked light reflectance increases. For the cone distribution to be mapped, subjects did not need to be dark adapted or to have their heads fixed by a dental impression mouthpiece. The total recording time was only the 12 s required for taking four consecutive photographs. For the recordings, the original fundus camera was minimally modified: the shape of the fixation target was changed from a circle to a triangle so that each subject could fixate on an apex to reduce eye movements during the recording. Both the apparatus and recording protocol appear to be the simplest of any developed version of imaging reflectometry.

The reflectance changes were induced by white flashes, and the raw images contained information on the blue, green, and red components of the image. However, the individual sensitivity of the commercial CMOS camera to these wavelengths was not available. In addition, the wavelength of peak sensitivity of each color did not match that of the short (S)-, middle (M)- and long (L)-wavelength cones, and the wavelength bands greatly overlap. For the analysis, the raw images were first transformed to TIFF images, ensuring the linearity of information on each color. The raw images obtained by this camera, however, are specially designed to show the color of the retinal components, such as of the retinal pigment epithelium, optic disc, and retinal vessels, as clearly as possible to be useful for diagnosis of retinal diseases. The core information on color-image processing has not been disclosed by the manufacturer. In fact, particular color information might be more weighted than that of other luminances for better observation of the retinal structures. Thus, the extracted information on the three luminances could not be used for differential mapping of the densities of the rods, and of the S-, M-, and L-wavelength cones. Moreover, the reflectance changes (%) shown in the results do not reflect the exact quantitative changes in photopigment bleaching because of postprocessing of the images before the raw images were obtained. In the future, replacement of the CMOS camera with a color CCD camera whose properties are provided by the manufacturer will allow us to map the density of the different types of photoreceptors without using band-pass interference filters.

In fundus camera-based imaging reflectometry, the appearance of a major artifact that arises from unwanted scattered light from the retinal surface is inevitable. Because of the high reflectivity of the inner limiting membrane and nerve fiber layer, especially around the macular region, minute eye movements between consecutive images may induce pseudo-light reflectance increases or decreases, which may mimic the bleaching topography. However, in the monkey's retina, the ratio of the reflectance of the central peak to the surroundings was high for the red and low for the blue and green images (Fig. 2). These results indicate that the cone photoreceptors contributed to the red image, and both cone and rod photoreceptors to the shorter wavelength images. Thus, the reflectivity changes measured by this method are not artifacts but are derived from changes in the density of photopigments in the photoreceptors.

The principle by which the bleached topography was extracted is exactly the same as that used in earlier reflectometry techniques. Thus, our results suffer from the same artifacts inherent in those methods.[31,32] First, artifacts are induced by movements of the retinal images during a recording session caused by head or eye movements. These are inherent in all of the reflectometry systems, and one of the best solutions is to reduce the time for data acquisition. In our system, the duration for data recording was less than 1.0 ms, determined by the duration of the xenon flash strobe. This short duration helped reduce movement artifacts and made off-line image registration easier. The short acquisition time, on the other hand, decreased the SNR, because we did not average data of different recording sessions. Our single-trial protocol, however, made the total recording time as short as 12 s, thus making this recording procedure more practical for clinical applications.

The second limitation of our technique is the inhomogeneous distribution of the light flash due to the optics of the fundus camera, where the light reaching the optical center is about three times as intense as that 15° from the center. The third limitation was the presence of scattered light from the inner limiting membrane and nerve fiber layer around the macula. The scattered light is a serious problem when examining the spatial distribution of reflectance changes, especially in younger subjects (Fig. 4, subjects 2 and 3). However, we examined the bleached topography of cones within the macular region, which is less vulnerable to such artifacts. When the bleached topography of the entire region within the vascular arcades is examined, such artifacts will be a more serious problem.

In conclusion, we took snapshots of the ocular fundus with a minimally modified commercial fundus camera and obtained topographic maps of the bleached cone photoreceptors in anesthetized monkeys and alert human subjects. This technique will potentially provide new methods for clinical measurements of photoreceptor function in both normal and diseased retinas.

*Acknowledgments.* We thank Prof. Mitsuko Yuzawa at Nihon University for special support of our studies and Prof. D. Hamasaki for his help in editing the manuscript. This research was supported in part by (1) research grants from the Ministry of Health, Labour and Welfare, Japan and (2) SENTAN, JST, Japan.

## References

1. Webb RH, Hughes GW. Scanning laser ophthalmoscope. IEEE Trans Biomed Eng 1981;28:488–492.
2. Mainster MA, Timberlake GT, Webb RH, Hughes GW. Scanning laser ophthalmoscopy. Clinical applications. Ophthalmology 1982; 89:852–857.
3. Huang D, Swanson EA, Lin CP, et al. Optical coherence tomography. Science 1991;254:1178–1181.
4. Hee MR, Izatt JA, Swanson EA, et al. Optical coherence tomography of the human retina. Arch Ophthalmol 1995;113:325–332.
5. Sutter EE, Tran D. The field topography of ERG components in man. I. The photopic luminance response. Vision Res 1992;32: 433–446.
6. Harary HH, Brown JE, Pinto LH. Rapid light-induced changes in near infrared transmission of rods in *Bufo marinus*. Science 1978;202:1083–1085.
7. Tsunoda K, Oguchi Y, Hanazono G, Tanifuji M. Mapping cone- and rod-induced retinal responsiveness in macaque retina by optical imaging. Invest Ophthalmol Vis Sci 2004;45:3820–3826.
8. Hanazono G, Tsunoda K, Shinoda K, Tsubota K, Miyake Y, Tanifuji M. Intrinsic signal imaging in macaque retina reveals different types of flash-induced light reflectance changes of different origins. Invest Ophthalmol Vis Sci 2007;48:2903–2912.
9. Inomata K, Tsunoda K, Hanazono G, et al. Distribution of retinal responses evoked by transscleral electrical stimulation detected by intrinsic signal imaging in macaque monkeys. Invest Ophthalmol Vis Sci 2008;49:2193–2200.
10. Hanazono G, Tsunoda K, Kazato Y, Tsubota K, Tanifuji M. Evaluating neural activity of retinal ganglion cells by flash-evoked intrinsic signal imaging in macaque retina. Invest Ophthalmol Vis Sci 2008;49:4655–4663.
11. Nelson DA, Krupsky S, Pollack A, et al. Special report: noninvasive multi-parameter functional optical imaging of the eye. Ophthalmic Surg Lasers Imaging 2005;36:57–66.
12. Abramoff MD, Kwon YH, Ts'o D, et al. Visual stimulus-induced changes in human near-infrared fundus reflectance. Invest Ophthalmol Vis Sci 2006;47:715–721.
13. Crittin M, Riva CE. Functional imaging of the human papilla and peripapillary region based on flicker-induced reflectance changes. Neurosci Lett 2004;360:141–144.
14. Tsunoda K, Hanazono G, Inomata K, Kazato Y, Suzuki W, Tanifuji M. Origins of retinal intrinsic signals: a series of experiments on retinas of macaque monkeys. Jpn J Ophthalmol 2009;53:297–314.
15. Yao XC, Yamauchi A, Perry B, George JS. Rapid optical coherence tomography and recording functional scattering changes from activated frog retina. Appl Opt 2005;44:2019–2023.
16. Bizheva K, Pflug R, Hermann B, et al. Optophysiology: depth-resolved probing of retinal physiology with functional ultrahigh-resolution optical coherence tomography. Proc Natl Acad Sci U S A 2006;103:5066–5071.
17. Srinivasan VJ, Wojtkowski M, Fujimoto JG, Duker JS. In vivo measurement of retinal physiology with high-speed ultrahigh-resolution optical coherence tomography. Opt Lett 2006;31: 2308–2310.
18. Rushton WA. The difference spectrum and the photosensitivity of rhodopsin in the living human eye. J Physiol 1956;134:11–29.
19. Hood C, Rushton WA. The Florida retinal densitometer. J Physiol 1971;217:213–229.
20. Rushton WA. Cone pigment kinetics in the protanope. J Physiol 1963;168:374–388.
21. Alpern M, Maaseidvaag F, Oba N. The kinetics of cone visual pigments in man. Vision Res 1971;11:539–549.
22. Alpern M. Rhodopsin kinetics in the human eye. J Physiol 1971;217:447–471.
23. Mizuno K, Majima A, Ozawa K, Ito H. Red-free light fundus photography. Photographic optogram. Invest Ophthalmol 1968;7:241–249.
24. Highman VN, Weale RA. Rhodopsin density and visual threshold in retinitis pigmentosa. Am J Ophthalmol 1973;75:822–832.
25. Sheorey UB. Clinical assessment of rhodopsin in the eye. Using a standard fundus camera and a photographic technique. Br J Ophthalmol 1976;60:135–141.
26. Kilbride PE, Read JS, Fishman GA, Fishman M. Determination of human cone pigment density difference spectra in spatially resolved regions of the fovea. Vision Res 1983;23:1341–1350.
27. Kilbride PE, Keehan KM. Visual pigments in the human macula assessed by imaging fundus reflectometry. Appl Opt 1990;29:1427–1435.
28. Faulkner DJ, Kemp CM. Human rhodopsin measurement using a T.V.-based imaging fundus reflectometer. Vision Res 1984;24: 221–231.
29. Kemp CM, Faulkner DJ, Jacobson SG. The distribution and kinetics of visual pigments in the cat retina. Invest Ophthalmol Vis Sci 1988;29:1056–1065.
30. van Norren D, van de Kraats J. Imaging retinal densitometry with a confocal scanning laser ophthalmoscope. Vision Res 1989;29: 1825–1830.
31. Elsner AE, Burns SA, Hughes GW, Webb RH. Reflectometry with a scanning laser ophthalmoscope. Appl Opt 1992;31:3697–3710.
32. Berendschot TT, DeLint PJ, van Norren D. Fundus reflectance—historical and present ideas. Prog Retin Eye Res 2003;22:171–200.
33. Osterberg G. Topography of the layer of rods and cones in the human retina. Acta Ophthalmol 1935;13:6–97.
34. Curcio CA, Sloan KR, Kalina RE, Hendrickson AE. Human photoreceptor topography. J Comp Neurol 1990;292:497–523.
35. Liem AT, Keunen JE, Van Norren D. Clinical applications of fundus reflection densitometry. Surv Ophthalmol 1996;41:37–50.
36. Elsner AE, Burns SA, Beausencourt E, Weiter JJ. Foveal cone photopigment distribution: small alterations associated with macular pigment distribution. Invest Ophthalmol Vis Sci 1998;39: 2394–2404.
37. Tornow RP, Beuel S, Zrenner E. Modifying a Rodenstock scanning laser ophthalmoscope for imaging densitometry. Appl Opt 1997;36:5621–5629.
38. Sekiryu T, Iida T, Maruko I, Horiguchi M. Clinical application of autofluorescence densitometry with a scanning laser ophthalmoscope. Invest Ophthalmol Vis Sci 2009;50:2994–3002.